Hybrid Synchronized PWM Schemes for Closed Loop Current Control of High Power Motor Drives

Haitao Yang, *Student Member, IEEE,* Yongchang Zhang, *Member, IEEE,* Guofeng Yuan, Paul D. Walker and Nong Zhang

***Abstract*—For high power drives, switching frequency is usually restricted to several hundred hertz to minimize the switching losses. To maintain the current distortions and torque ripples at a reasonable level, synchronized pulse patterns with half-wave and quarter-wave symmetries are employed. The analytic compensation is derived by Fourier analysis to ensure the proportionality between the voltage reference and the output voltage of an inverter for PWM with low pulse ratio. A simple yet very effective method with varying sampling rate is proposed to maintain synchronization even for fast dynamic processes. The fast and smooth transition between different PWM patterns is achieved by compensating phase angle of the voltage reference through the analysis of stator flux trajectories. The effectiveness of the proposed method is validated on a down-scaled 2.2 kW induction motor (IM) drives.**

***Index Terms*—Field-oriented control (FOC), hybrid PWM, high-power motor drives, synchronous PWM**

NOMENCLATURE

Symbols

$\boldsymbol{i}$	Current Vector
$\boldsymbol{u}$	Voltage Vector
$\boldsymbol{\psi}$	Flux Vector
L, R	Inductance and resistance
ω	Angular frequency
T	Time
j	Imaginary part of a complex variable
s	Laplace operator
z	Discrete-time operator
k	Gain
M	Modulation index
P	Pulse ratio
α, β	Angle of the complex vector
p	Derivative operator

Subscripts

s, m, r	Stator, mutual, and rotor
d, q	d and q axes
dc	DC link
c	Continuous-time domain
d	Discrete-time domain

Superscripts

e	Synchronous reference frame
ref	Reference value
inv	Output of the inverter

I. INTRODUCTION

For high-power drives, operating at low switching frequency for inverters is mandatory to restrain switching losses. However, maintaining satisfactory performance at lower switching frequency brings many challenges. The pulse ratio, namely the pulse number during one fundamental cycle, is very low in high-power applications. Thus, if the popular space vector modulation (SVM) or carrier based sinusoidal PWM (SPWM) is adopted, the unacceptable current distortion including large low order harmonics and sub-harmonics can be seen in the spectrum analysis [1]. This would lead to larger loss, higher torque ripples, poorer current regulation bandwidth, etc. To address these problems, various PWM schemes have been proposed. Generally, the pulse ratio is kept constant over a speed range to eliminate the sub-harmonics, namely that it is synchronized with the output frequency of the inverter. With the continuous efforts of many researchers, synchronized SPWM, synchronized SVPWM, selective harmonic elimination PWM (SHEPWM) and current harmonic minimum PWM (CHMPWM), have been applied in practical applications [1]–[5].

To keep half-wave symmetry (HWS), quarter-wave symmetry (QWS), and three phase symmetry (TPS) in synchronous SPWM and SVPWM, the pulse ratio has to be odd integer multiples of 3. Large variation of the switching frequency can be observed for variable speed drives due to the limited selection of the pulse ratio. The space vector based PWM schemes can offer some flexibilities, such as division of zero state duration and clamping one phase within a PWM interval. Utilizing these flexibilities, some advanced PWM schemes can be developed to improve the harmonic performance [6], reduce the torque ripple [7], design the synchronized symmetric PWM strategies for higher power drivers [3], [8], and so on. In [9], different synchronized PWM schemes are studied, but only the results of V/f operation are presented. In [2], the carrier based synchronized PWM is incorporated with FOC, showing good dynamic and steady state performance. However, the extraction of current harmonics is based on a leakage model, of which the machine parameters tend to vary depending on the temperature and saturation [10]. Consequently, to ensure the estimated current harmonic is in accordance with actual value in practical application, online adaption algorithm may be required.

SHEPWM and CHMPWM have also been widely studied and applied owing to their superior harmonic performance [4], [5], [11], [12]. For those PWM techniques, complex

mathematical skills and calculating programs are usually required to obtain the optimal switching angles [12], [13]. To meet the demands of accuracy and cover a wide speed range operation, numerous results should be optimized offline and stored for online implementation. As those PWM techniques may introduce discontinuities in the switching angles and the flux/current trajectory may not coincide with each other at the same sampling point for different pulse patterns, high dynamic closed-loop control systems based on SHEPWM and CHMPWM are usually complicated.

To satisfy the demand over a wide speed range, a combination of PWM schemes with different pulse patterns are usually used. This imposes the requirement of smooth transition between different PWM methods. In [5], the transition is enabled when the voltage angle falls into a fixed range. But the selection of this range is not clearly addressed with theory analysis. In [14], the transition is started when the harmonic current is around zero. It is shown that the transition is smooth. However, the gate pulses of three phases are shifted separately at different points, increasing the complexity and duration of PWM shifting process. To improve the overall performance, SHEPWM is employed in [4] during steady state operation while it is switched to SVPWM during dynamic process. The smooth transition is achieved by optimizing the switching state so that there is no more than one pulse jump during transition. As the the pulse number is as high as 29 in quarter fundamental cycle, the harmonic current is very small and nearly zero. According to [14], the transition can be started at any positions. Since operation with low switching frequency presents abundant harmonic components, this method is not applicable when the pulse number is low. In [1], [15], the dynamic error caused by transition between different pulse patterns is combined with the tracking error induced by load change, reference variation, etc. All these disturbances are compensated in the controller by directly manipulating original switching instants according to the tracking error of stator flux. As the problem of achieving smooth transition is solved in the design of controller, it is applicable for various pulse patterns. In this paper, the dynamic error induced by transition between different pulse patterns will not be compensated in the controller but solved in the modulation stage. In this way, the controller design and modulation schemes are decoupled. Namely, it is not necessary for inner current controller to consider the effect of shifting between different pulse patterns. Thus, the proposed method can be easily implemented with existing current controllers.

The main contribution of this paper is to decouple the inner current controller from various issues caused by implementation of synchronized PWM schemes. On this basis, the space vector and bus-clamping based synchronized PWM are employed without the requirement of fundamental current estimation. The linearity between the reference voltage and the output voltage is guaranteed by analyzing the PWM sequence through Fourier analysis. Methods to keep synchronization and schemes for smooth transition between different pulse patterns are proposed and elaborated in detail by analytic derivation. The experimental results on a down-scaled IM drive platform validate the effectiveness of the proposed methods.

TABLE I
SYNCHRONOUS PWM SCHEMES

P	Position of samples in sector 1	Vector Sequences in sector 1
15	6°, 18°, 30°, 42°, 54°	0127, 7210, 0127, 7210, 0127
11	6°, 18°, 30°, 42°, 54°	012, 210, 0127, 721, 127
7	10°, 30°, 50°	127, 7210, 012
3	30°	0127

II. MODEL OF IM

Considering the discrete nature of the digital control system, a discrete-time domain transfer function in the rotor flux oriented synchronous frame is derived in [16] with time delay T_d as

$$\frac{\boldsymbol{i}_s^e(z)}{\boldsymbol{u}_s^e(z)} = \frac{(1-e^{-(R_\sigma/L_\sigma)T_{sc}})}{R_\sigma \cdot z \cdot e^{j\omega_e T_d} \cdot (z \cdot e^{j\omega_e T_{sc}} - e^{-(R_\sigma/L_\sigma)T_{sc}})} \quad (1)$$

$$T_\sigma = \frac{\sigma L_s}{R_s + (L_m/L_r)^2 R_r} \quad (2)$$

$$\sigma = \frac{L_s L_r - L_m^2}{L_s L_r} \quad (3)$$

where T_{sc} is the sampling period, $L_\sigma = \sigma L_s$, $R_\sigma = R_s + (L_m/L_r)^2 R_r$.

Considering the compensation of time delay, the discrete current controller can be developed as (4) based on (1) as [16]

$$G_d(z) = k_d \frac{e^{j\omega_e T_{sc}} - z^{-1} \cdot e^{-(R_\sigma/L_\sigma)T_{sc}}}{(1-z^{-1})} e^{j\omega_e T_d} \quad (4)$$

III. HYBRID PWM SCHEMES

For a two-level inverter, there are two zero vectors and six different active vectors, dividing the complex plane into six sectors, as shown in Fig. 1. For satisfying the requirements over the whole speed range, the hybrid PWM schemes with different pulse ratios are usually employed. In this paper, the following PWM schemes, synchronous SVPWM with $P = 15, 3$ and basic bus clamping strategy-I (BBCS-I) PWM with $P = 11, 7$ are selected according to [3], [8]. For simplicity, they are named as SVPWM_15, SVPWM_3, BBCS_11 and BBCS_7 respectively in the following text. The vector sequences of these PWM schemes during sector 1 are listed in Table I. More characteristics about these PWM schemes can be found in [3], [8], [17]. An illustration of the relationship between the modulation index, switching frequency and the fundamental frequency is shown in Fig. 2. According to Table I, two conditions should be satisfied to generate desired pulse shapes. The first one is that the phase angle of voltage vector must equal the sampling positions defined in the second column. The second one is that the voltage vector at these sampling positions should be synthesized by the corresponding vector sequences as shown in the third column. The modulation index here is defined as

$$M^{ref} = \frac{\sqrt{3} u_s^{ref}}{U_{dc}} \quad (5)$$

Before these PWM methods are employed in closed-loop control system, some issues must be solved. Firstly, the

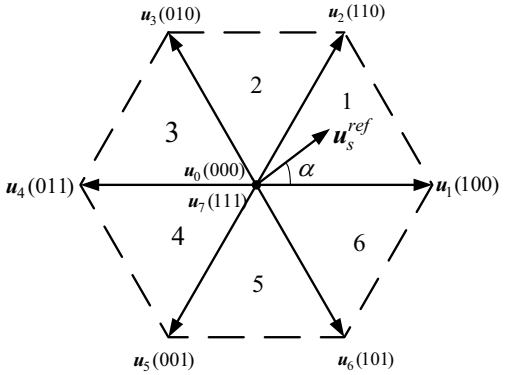

Fig. 1. Illustration of voltage vectors and 6 sectors

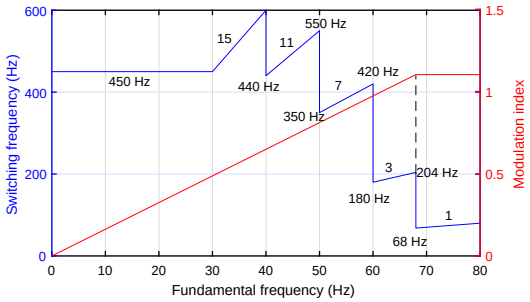

Fig. 2. Diagram of the relationship between the modulation index, switching frequency and the fundamental frequency

synchronization must be well kept in both steady and dynamic process. Secondly, the smooth and fast transition between different PWM schemes should be achieved to avoid current/torque oscillations. Thirdly, the output fundamental voltage of the inverter must coincide with the reference voltage. Because the reference voltage is usually used in the observer to get the information of flux. Finally, stable and fast control of stator current should be guaranteed under low switching frequency operation. The following text will present some methods to cope with these problems. It is assumed in this paper that both the current sampling and PWM updating instant are synchronized with the sampling position as shown in the second column of Table I. This is based on the consideration that there is no switching transition at these sampling position and thus the current sampling would not be polluted by switching noise. Additionally, the selected PWM schemes are space vector based methods, the acquisition of fundamental current is permitted at the end of each subcycle [1]. This makes control of stator current without fundamental component estimation possible. Another benefit is that, as the current sampling is synchronized with PWM updating instant, it is easier to analyze and handle the modulation delay based on previous researches, such as [16], [18].

A. Synchronization Scheme

To maintain synchronization, two following steps are taken. The first step is to set a proper PWM updating frequency f_{pwm} to keep the pulse ratio constant over a speed range, which are $30f_e$, $30f_e$, $18f_e$ and $6f_e$ for SVPWM_15, BBCS_11, BBCS_7 and SVPWM_3 respectively. The second step is to match the PWM updating instant. During the steady state, the voltage vector rotates in the complex plane smoothly. Thus, if the first step is implemented, the increment of the angle of the voltage vector will always be the same. Take the SVPWM_15 as an example, if the starting position of the voltage vector is $6°$, then the following phase angles of the voltage vector would be $6° + k \cdot 12°$ $(k = 1, 2, 3...)$. However, in the closed-loop system, the phase angle of the voltage vector θ_u may vary sharply at any time, it is difficult to keep θ_u matching the sampling position shown in Table I. To address this problem, the PWM interval set in the first step is compensated in a deadbeat fashion to correct the mismatch. Take SVPWM_15 as an example to clarify this point, the difference of the phase angle between θ_u and the sampling position shown in Table I is calculated at each starting instant of the PWM interval as

$$\theta_{err} = \theta^{ref} - \theta_u \tag{6}$$

Where $\theta_u = \text{angle}(\boldsymbol{u}_s)$ (degree), $\theta^{ref} = 12k + 6$, $k = \text{round}\left((\theta_u - 6)/12\right)$. It is clear that to cancel θ_{err}, the compensation of the time required is

$$T_{com} = \frac{\pi\theta_{err}}{180} \cdot \frac{1}{2\pi f_e} = \frac{\theta_{err}}{360 f_e} \tag{7}$$

After obtaining T_{com}, the PWM updating interval for SVPWM_15 is

$$T_{pwm} = \frac{1}{30 f_e} + T_{com} \tag{8}$$

For the synchronization of other PWM schemes, the same method is applied. As the compensation is performed in a deadbeat fashion, any mismatch will be corrected in one PWM interval. Thus keeping synchronization during fast dynamic process can be ensured.

B. Keeping Linearity between Reference and Output

With very low pulse ratio of 3, the relationship between actual modulation index of the invert output voltage and u_s^{ref} may be not linear. In this paper, the compensation for linearity and overmodulation is investigated directly by analyzing PWM sequences. It is found that the gain compensation is required for SVPWM_3 and analytic solution is derived in order to avoid using lookup tables.

For space vector based PWM, the reference voltage vector in each sector can be synthesized by two adjacent active vectors $\boldsymbol{u}_x$ and $\boldsymbol{u}_y$, and one or two zero vectors, with their respective duty ratio calculated as

$$d_x = M^{ref} \cdot \sin(60° - \alpha) \tag{9}$$

$$d_y = M^{ref} \cdot \sin\alpha \tag{10}$$

$$d_0 = 1 - d_1 - d_2 \tag{11}$$

where α is the angle between $\boldsymbol{u}_s^{ref}$ and $\boldsymbol{u}_x$.

Fig. 3 shows the pole voltage of SVPWM_3 in the range of $0° \sim 90°$ of the stator flux trajectory depicted in Fig. 4d. According to (9)-(11), the angle β can be obtained as

$$\beta = 30° \cdot \left\{1 - M^{ref}\right\}. \tag{12}$$

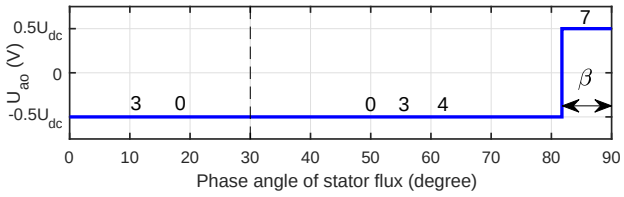

Fig. 3. Pole Voltage of phase 'a' and corresponding vector number for SVPWM_3

TABLE II
MODIFIED SCHEME OF SVPWM_3

P	Position of samples in sector 1	Vector Sequences in sector 1
3	10°, 30°, 50°	01, 12, 27

Then, the output fundamental voltage can be expressed as [12]

$$U = \frac{2U_{dc}}{\pi}\left[1 - 2\sin\beta\right]$$

Thus, the actual output modulation index of the inverter voltage for SVPWM_3 is

$$M_3^{inv} = \frac{2\sqrt{3}}{\pi}\left[1 - 2\sin\beta\right]. \tag{13}$$

Based on (13), to make the M_3^{inv} equal to M^{ref}, the original M^{ref} in (12) should be modified as

$$M_{mod}^{ref} = \frac{30° - \arcsin(0.5 - \sqrt{3}\pi M^{ref}/12)}{30°}. \tag{14}$$

After the modulation index M^{ref} is obtained from the output of the current controller using (5), a modified virtual modulation index M_{mod}^{ref} should be calculated based on (14). Then, the duty ratio of each voltage vector can be calculated according to (9)-(11) using M_{mod}^{ref} instead of M^{ref}. It should be noted that as the deduction of (14) is directly based on mathematical analysis, it is precise for the whole range of M^{ref}, including over modulation.

Additionally, the original vector sequence in SVPWM_3 is modified and the sampling rate is increased to 18 times of the fundamental frequency to reduce time delay. Take the sector 1 as an example, the original vector sequence 0127 accounts for 60° as shown in Table I will be modified as 01, 12, 27 with each sequence accounts for 20°. After this modification, the whole vector sequence for every 60° is still the same as the original. But the sampling frequency can be improved to $18f_e$. This would bring some benefits to the current closed-loop control, such as lower sampling delay and higher controller bandwidth. The modified vector sequences are listed in Table II. It should be noted that the duration of each voltage vector should be kept the same as the original to produce the same output. According to (11), the duration of zero vector can be calculated as

$$T_0 = \frac{1 - M_{mod}^{ref}}{6f_e}. \tag{15}$$

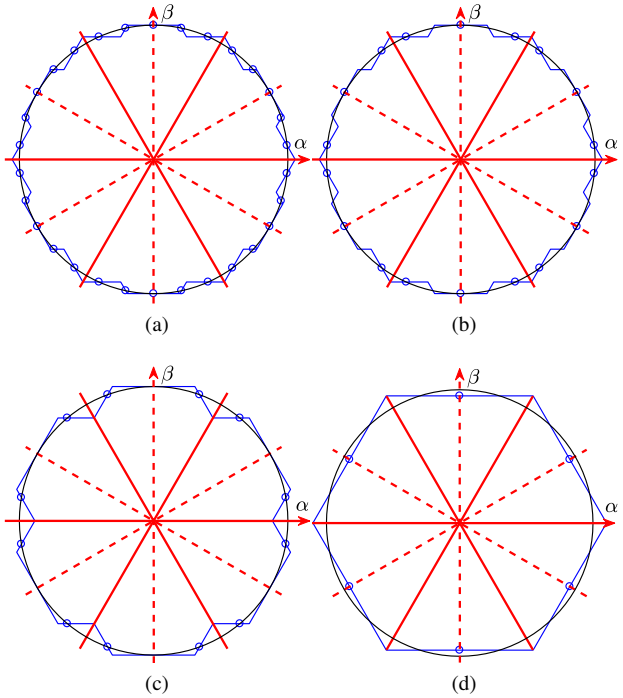

Fig. 4. Flux trajectories for (a) SVPWM_15, (b) BBCS_11, (c) BBCS_7 and SVPWM_3

Considering that T_0 is divided equally for $\boldsymbol{u}_0$ and $\boldsymbol{u}_7$, the duration of the active vector $\boldsymbol{u}_1$ can be calculated as (16) when the sampling position of 10° is considered in this example.

$$T_1 = \frac{1}{18f_e} - 0.5T_0 = \frac{3M_{mod}^{ref} - 1}{36f_e} \tag{16}$$

The duration of an active vector combining with a zero vector at other sampling positions can be calculated in the same way. When the sampling position is $30°, 90°...330°$, both active voltage vectors account for $1/(36f_e)$.

C. Transition Strategy

As the current/flux trajectory of the PWM pattern is different from each other, the transition strategy should be carefully designed to avoid dynamic error which may cause torque oscillation and over-current event. In this paper, the transition strategy is designed based on the analysis of flux trajectories of different PWM schemes. To achieve smooth transition, the original voltage reference will be compensated by a complex gain so that the end point of flux trajectory will be located on the new flux trajectory after the transition. As discontinuities of stator flux trajectory due to the transition between different PWM patterns is compensated using this method, there would be no dynamic error and thus the transition would be smooth and fast [19].

The flux trajectory can be obtained according to the vector sequence listed in Table I by integration, and they are shown in Fig. 4. The small circles in the figures indicating that there is a zero vector and the flux vector $\boldsymbol{\psi}_s$ is stationary at those positions until an active vector is applied.

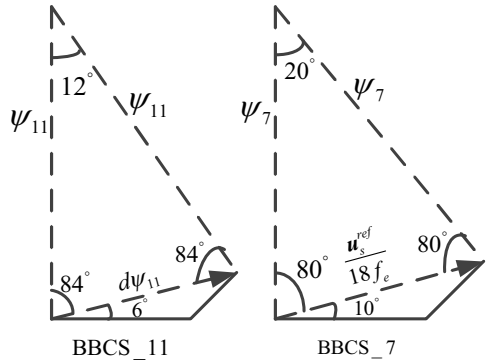

Fig. 5. Illustration of flux trajectories of BBCS_11 and BBCS_7 during one subcycle

1) Transition between conventional SVPWM and SVPWM_15: Transition between asynchronous SVPWM and SVPWM_15 is relatively easy. As both PWM schemes are traditional SVPWM, harmonic current is zero at the end of each subcycle. Thus, the transition can be started at the beginning of each PWM interval [14]. It should be noted that, though the phase angle of the voltage vector at the transition instant may be not the same as those listed in the Table I when transferring to SVPWM_15, the synchronization scheme described in Section III-A will help to setup the match with these positions and thus the symmetry of the output voltage can be well maintained.

2) Transition between SVPWM_15 and BBCS_11: It can be seen from Table I that the sampling position of BBCS_11 is the same as SVPWM_15, and there is only difference in the use of zero vectors for generating vector sequences. As the zero vector does not alter the flux vector, the flux trajectory of BBCS_11 should be the same as that of SVPWM_15. This can be clearly seen in Fig. 4. It is obvious that there are more zero vectors in SVWPM_15 and the shapes of flux trajectory of SVPWM_15 and BBCS_11 are same. This indicates that the transition between SVPWM_15 and BBCS_11 can be started at any sampling position, because the flux trajectory coincides with each other. Hence, there is no dynamic error when the transition between SVPWM_15 and BBCS_11 happens.

3) Transition between BBCS_11 and BBCS_7: The stator flux vector rotates $12°$ and $20°$ for BBCS_11 and BBCS_7 during their respective subcycle. The Fig. 5 shows the flux trajectory in the subcycle of $270° \sim 282°$ and $270° \sim 290°$ for BBCS_11 and BBCS_7 respectively. The corresponding sampling positions of voltage are $6°$ and $10°$ respectively. Then, ψ_{11} in Fig. 5 can be simply calculated according to the law of sines as follows.

$$\frac{\psi_{11}}{\sin(84°)} = \frac{d\psi_{11}}{\sin(12°)} \tag{17}$$

The time of every subcyle of BBCS_11 is $1/(30f_e)$, thus $d\psi_{11}$ is

$$d\psi_{11} = \frac{\left|\boldsymbol{u}_s^{ref}\right|}{30f_e}. \tag{18}$$

where $|\bullet|$ represents the magnitude of the complex vector. Based on above two equations, ψ_{11} is obtained as

$$\psi_{11} = \frac{\sin(84°)}{\sin(12°)} \cdot \frac{\left|\boldsymbol{u}_s^{ref}\right|}{30f_e}. \tag{19}$$

Similarly, ψ_7 can be deduced as

$$\psi_7 = \frac{\sin(80°)}{\sin(20°)} \cdot \frac{\left|\boldsymbol{u}_s^{ref}\right|}{18f_e} \tag{20}$$

When a transition from BBCS_11 to BBCS_7 occurs, the original reference vector $\boldsymbol{u}_s^{ref}$ should be multiplied by a complex compensation gain $\boldsymbol{k}_{11\_7}$ to make the flux vector rotates from $\psi_{11} \cdot e^{j\cdot 270°}$ to $\psi_7 \cdot e^{j\cdot 290°}$ at the end of the transition. Thus, $\boldsymbol{k}_{11\_7}$ can be calculated as follows

$$\boldsymbol{k}_{11\_7} \cdot \boldsymbol{u}_s^{ref} = \left(\psi_7 \cdot e^{j\cdot 290°} - \psi_{11} \cdot e^{j\cdot 270°}\right) \cdot 18f_e \tag{21}$$

As $\boldsymbol{u}_s^{ref} = \left|\boldsymbol{u}_s^{ref}\right| e^{j\cdot 6°}$ in this subcyle for BBCS_11, $\boldsymbol{k}_{11\_7}$ can be obtained from (21) as

$$\boldsymbol{k}_{11\_7} = \left\{\frac{\sin(80°)\cos(70°)}{\sin(20°)} - j \cdot A\right\} e^{-j\cdot 6°} \tag{22}$$

$$A = \frac{0.6\sin(84°)}{\sin(12°)} - \frac{\sin(80°)\sin(70°)}{\sin(20°)} \tag{23}$$

It can be found that the expression of $\boldsymbol{k}_{11\_7}$ is somewhat complicated. Fortunately, it is a fixed value independent of any parameters. Thus an approximate numerical solution of $\boldsymbol{k}_{11\_7}$ can be calculated offline and used in practical application, which is

$$\boldsymbol{k}_{11\_7} \approx e^{j\cdot 3.47°} \tag{24}$$

It turns out that the phase angle of $\boldsymbol{u}_s^{ref}$ should be compensated by $3.47°$ when transferring from BBCS_11 to BBCS_7 at the voltage vector sampling position of $6°$. The conclusion is valid for all transitions beginning at $60° \cdot k - 54°$ ($k = 1, 2...6$). Thus, there are 6 points where the transition from BBCS_11 to BBCS_7 can be started with the proposed method.

Similarly, the transition from BBCS_7 to BBCS_11 can be started at sampling position $60° \cdot k - 50°$ ($k = 1, 2...6$) and the complex gain $\boldsymbol{k}_{7\_11}$ can be obtained as

$$\boldsymbol{k}_{7\_11} = \left\{\frac{\sin(84°)\cos(78°)}{\sin(12°)} - j \cdot B\right\} e^{-j\cdot 10°}, \tag{25}$$

$$B = \frac{\sin(80°)}{0.6 \cdot \sin(20°)} - \frac{\sin(84°)\sin(78°)}{\sin(12°)}. \tag{26}$$

The approximate numerical solution of $\boldsymbol{k}_{7\_11}$ is calculated as follow.

$$\boldsymbol{k}_{7\_11} \approx e^{-j\cdot 3.11°} \tag{27}$$

From (27), $3.11°$ should be subtracted from the phase angle of $\boldsymbol{u}_s^{ref}$ when transferring from BBCS_7 to BBCS_11.

4) Transition between BBCS_7 and SVPWM_3: Fig. 6 shows the trajectories of flux vector in the range of $270° \sim 330°$ for BBCS_7 and SVPWM_3, covering the sampling positions of $10°, 30°$ and $50°$ as listed in Table II. The θ in the figure represents the rotating angle of the flux vector within first subcyle. For SVPWM_3, it takes a time of $1/(6f_e)$ for

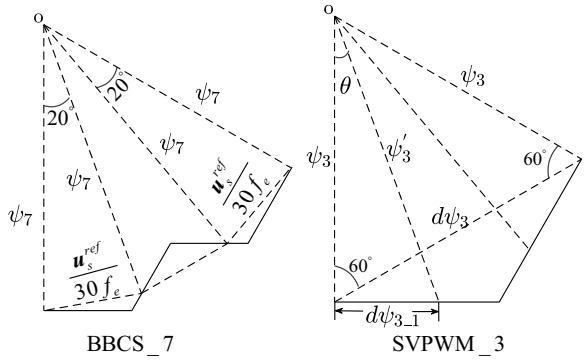

Fig. 6. Flux trajectories of BBCS_7 and SVPWM_3 during $270° \sim 330°$

stator flux rotates from 270° to 330°. According to (5) and (14), the $d\psi_3$ in Fig. 6 can be calculated as follows.

$$\begin{aligned} d\psi_3 &= \left|\psi_3 e^{j330^\circ} - \psi_3 e^{j270^\circ}\right| \\ &= \frac{M_{mod}^{ref} \cdot U_{dc}}{\sqrt{3}} \cdot \frac{1}{6f_e} \\ &= \frac{M_{mod}^{ref}}{M^{ref}} \cdot \frac{\left|\boldsymbol{u}_s^{ref}\right|}{6f_e} \end{aligned} \tag{28}$$

It can be found from Fig. 6 that ψ_3 is equal to $d\psi_3$. Hence, ψ_3 can be obtained as

$$\psi_3 = \frac{M_{mod}^{ref}}{M^{ref}} \cdot \frac{\left|\boldsymbol{u}_s^{ref}\right|}{6f_e}. \tag{29}$$

Based on (16), the $d\psi_{3\_1}$ in Fig. 6 can be deduced as

$$d\psi_{3\_1} = \frac{2}{3} U_{dc} \cdot T_1 = \frac{\sqrt{3}\left(3M_{mod}^{ref} - 1\right)}{M^{ref}} \frac{\left|\boldsymbol{u}_s^{ref}\right|}{54f_e}. \tag{30}$$

After obtaining ψ_3 and $d\psi_{3\_1}$, $\psi_3^{'}$ can be calculated as

$$\psi_3^{'} = \sqrt{(\psi_3)^2 + (d\psi_{3\_1})^2} \tag{31}$$

And θ can be obtained as

$$\theta = \arctan(\frac{d\psi_{3\_1}}{\psi_3}) \tag{32}$$

In this paper, SVPWM_3 is employed when $M^{ref} > 1$. Namely that, the transition between BBCS_7 and SVPWM_3 would begin at $M^{ref} = 1$. As shown in Table II, the sampling positions of the SVPWM_3 are the same as those of BBCS_7 after modification. Thus, if there is a position where the flux trajectories of two PWM schemes coincide with each other, the transition can be started and then the stator flux vector will follow the new one without error. To achieve this, the reference of voltage vector is first compensated by $\boldsymbol{k}_{7\_3}$ for BBCS_7 to cancel the error of flux vector and then the transition is started at the next sampling position. For example, if the transition begins at sampling position of 50°, the compensation stage should be performed at 30° . And, $\boldsymbol{k}_{7\_3}$ can be calculated as follows.

$$\frac{\boldsymbol{k}_{7\_3}\left|\boldsymbol{u}_s^{ref}\right| e^{j30^\circ}}{18f_e} = \psi_3^{'} e^{j(330^\circ - \theta)} - \psi_7 e^{j310^\circ} \tag{33}$$

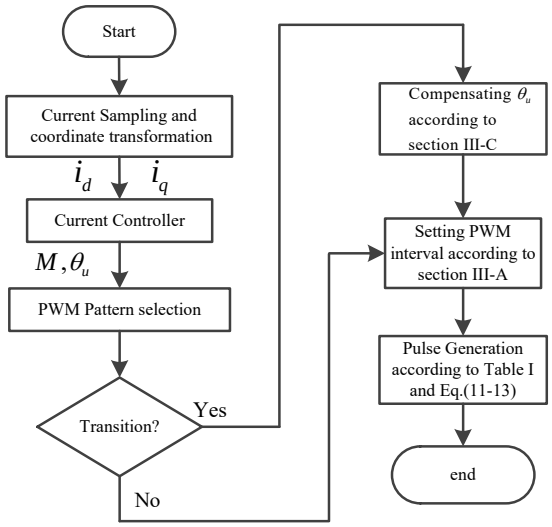

Fig. 7. Flowchart of the proposed method

Based on (20), (31) and (33), $\boldsymbol{k}_{7\_3}$ is obtained when $M^{ref} = 1$ as

$$\boldsymbol{k}_{7\_3} \approx e^{-j1.82^\circ}. \tag{34}$$

It is shown that only the phase angle of $\boldsymbol{u}_s^{ref}$ should be compensated by $-1.82°$. Then, the smooth transition from BBCS_7 to SVPWM_3 can be triggered at the next PWM interval. Due to the symmetry, the conclusion is valid for all transition at sampling position of $60°k - 10°$ $(k = 1, 2...6)$. In summary, the phase angle of $\boldsymbol{u}_s^{ref}$ is first compensated by $-1.82°$ at the sampling position $60°k - 30°$, then the output vector sequence is shifted from BBCS_7 to SVPWM_3 at the sampling position of $60°k - 10°$.

Similarly, the compensation gain of $\boldsymbol{k}_{3\_7}$ can be obtained as (35) when transferring from SVPWM_3 to BBCS_7 at the sampling position of $60°k - 10°$.

$$\boldsymbol{k}_{3\_7} \approx e^{j1.7^\circ} \tag{35}$$

Unlike other transition schemes, there are two steps for transferring from BBCS_7 to SVPWM_3, because the desired voltage vector can not be synthesized by the individual vector sequence shown in Table II. As a result, the compensation has to be implemented in BBCS_7 before entering SVPWM_3.

It should be noted that the concept of flux trajectory here is only used for analysis, but not used in the control system. The flowchart of the proposed method is shown in Fig. 7.

IV. Simulation and Experimental Tests

A. Simulation Results

In this section, the proposed method is simulated in the environment of MATLAB/Simulink based on a 180 kW IM with parameters listed in Table III. In simulation studies, results are obtained based on the control diagram shown in Fig. 8. To show the effectiveness of the proposed method, transition from BBCS_11 to BBCS_7 is simulated as an example. The results of closed-loop operation with current controller (4) are recorded in Fig. 9. The variable $flag$ in the figure represents different PWM schemes used in the control system. The value

TABLE III
PARAMETERS OF TESTED IMS

Rated power	P_N	2.2 kW	180 kW
DC-bus voltage	U_{dc}	540 V	1500 V
Rated voltage	U_N	380 V	1100 V
Rated frequency	f_N	50 Hz	60 Hz
Number of pole pairs	N_p	2	2
Stator resistance	R_s	1.76 Ω	0.09 Ω
Rotor resistance	R_r	1.29 Ω	0.065 Ω
Mutual inductance	L_m	0.158 H	0.038 H
Stator inductance	L_s	0.170 H	0.0394 H
Rotor inductance	L_r	0.170 H	0.0397 H

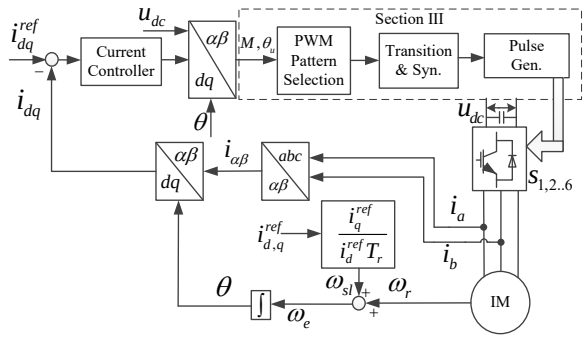

Fig. 8. Control diagram of the proposed scheme

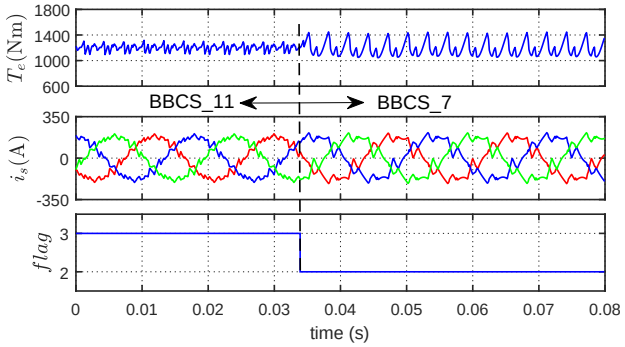

(a)

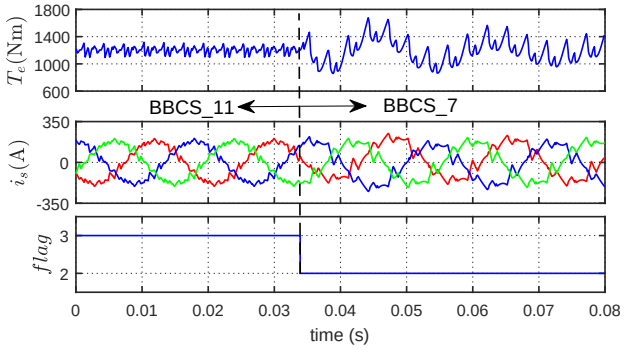

(b)

Fig. 9. Simulated responses during transition from BBCS_11 to BBCS_7 (a) with proposed transition scheme and (b) without proposed method

of $flag$ is one of $5, 4, 3, 2, 1$, which represents conventional SVPWM, SVPWM_15, BBCS_11, BBCS_7 and SVPWM_3 respectively. It is clear that smooth transition can be achieved without any oscillation and distortion when the proposed method is applied. While without the proposed method, there is an obvious torque excursion.

B. Experimental Results

The proposed method is implemented on a 32-bit floating point DSP TMS320F28335 and tested on a 2.2 kw IM platform. Motor parameters are listed in Table III. The control diagram of the proposed scheme is shown in Fig. 8. During the following tests, steady state and dynamic behavior of the current loop is the main performance of concern, and some other aspects such as the implementation of field weakening [20] are not demonstrated here.

Fig. 10 shows the responses during transition between different PWM schemes. Current and gate pulses plotted in these figures are directly measured by probe while the information of other variables are obtained via on-board DA converter. From top to bottom in each figure, the curves are a-phase gate pulses, i_q, a-phase current and variable $flag$ representing different PWM schemes. From results it can be seen that the symmetry of the gate pulse is well maintained for each synchronous PWM method and the transition is fast and smooth without inducing any obvious dynamic error.

Fig. 11 shows line voltages and corresponding weighted total harmonic distortion (WTHD) for different PWM strategies. WTHD is calculated as

$$U_{\text{WTHD}} = \frac{\sqrt{\sum (U_n/n)^2}}{U_1},\ n \neq 1. \tag{36}$$

where, U_1 and U_n are the root mean square values of the fundamental and nth harmonic voltages, respectively. It can be seen that the waveforms of line voltage are symmetry. There are no obvious sub-harmonics in line voltage and discrete nontriplen-odd-order harmonic components are distinctly identifiable, indicating that the pulse ratio is well synchronized with the operating speed.

As current deviation may be corrected by the closed-loop controller, the open loop test were also carried out, in order to clearly justify that the smooth transition can be achieved with only transition schemes. Fig. 12 shows the results during transition from BBCS_11 to BBCS_7. It is clear that there is a large current excursion during transition if the proposed method is not applied. This test confirms the effectiveness of the proposed method for achieving smooth transition.

Fig. 13 shows the dynamic performance when speed reference steps from 15 rpm to 1500 rpm. During the whole dynamic process, i_d is constant regardless of the variation of i_q, justifying that decoupling control of flux and torque is well achieved. It is also clear that the transitions between different PWM strategies are smooth without introducing any oscillation in i_d or i_q.

To verify the current control quality when the pulse ratio is low, the dynamic performance of i_q step response is tested and plotted in Fig. 14 when $P = 7$ and $P = 3$. It is seen that the shape of gate pulse is symmetry during both steady state and dynamic process, validating the effectiveness of the proposed synchronization strategy. The actual current can track the reference quickly and the settling time are about 12 ms and 15 ms for BBCS_7 and SVPWM_3 respectively. These

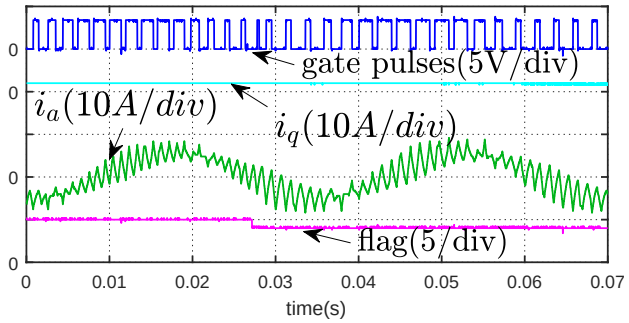

(a) Transition from conventional SVPWM to SVPWM_15

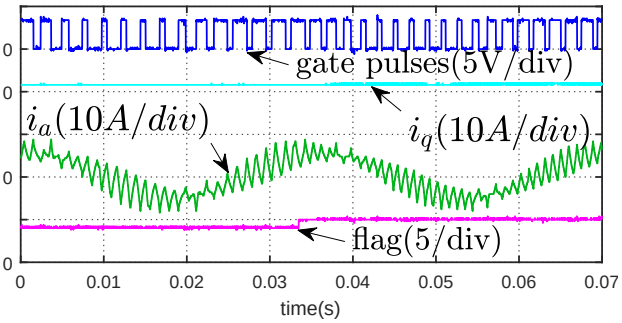

(b) Transition from SVPWM_15 to conventional SVPWM

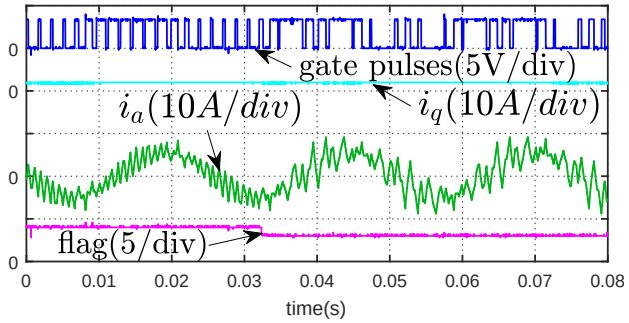

(c) Transition from SVPWM_15 to BBCS_11

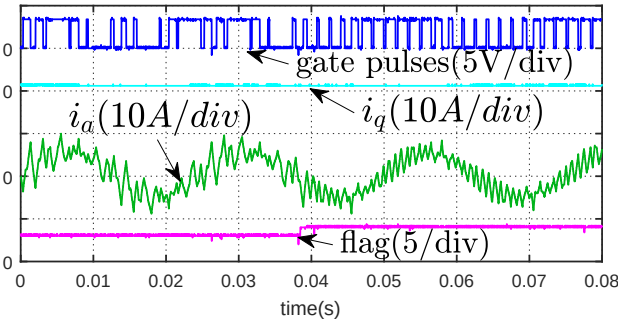

(d) Transition from BBCS_11 to SVPWM_15

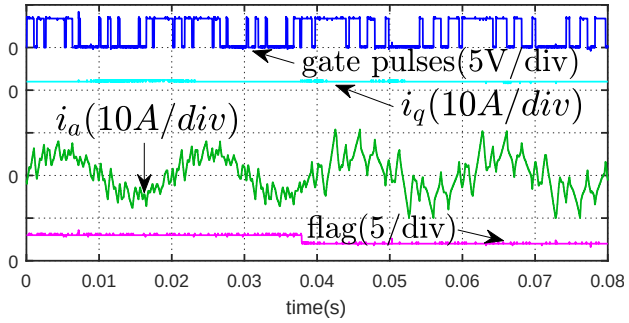

(e) Transition from BBCS_11 to BBCS_7

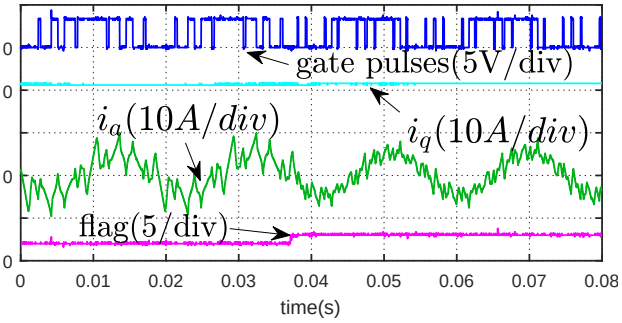

(f) Transition from BBCS_7 to BBCS_11

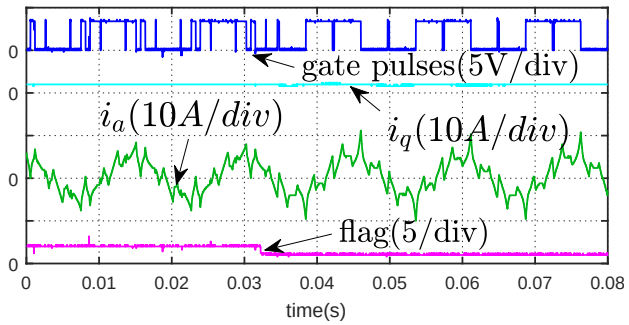

(g) Transition from BBCS_7 to SVPWM_3

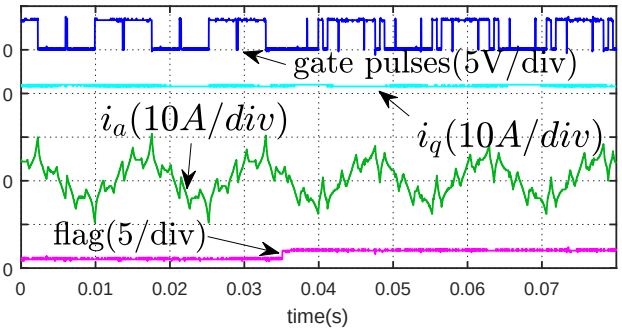

(h) Transition from SVPWM_3 to BBCS_7

Fig. 10. Closed-loop test results of transition between different PWM schemes

dynamic tests show that the whole regulation loop works well even when the pulse ratio is as low as 3. For achieving fast dynamic response, controller is one of the key factor. It is well known that the dynamic response of PI controller is not as good as that of direct torque control and predictive control [21]. To achieve faster dynamic response, other controllers, such as deadbeat predictive controller, can be investigated in future work.

V. Conclusion

This paper introduces an implementation of closed-loop current control based on hybrid synchronous PWM schemes for high power drives. A method by compensating phase angle of the voltage reference is deduced in detail to achieve

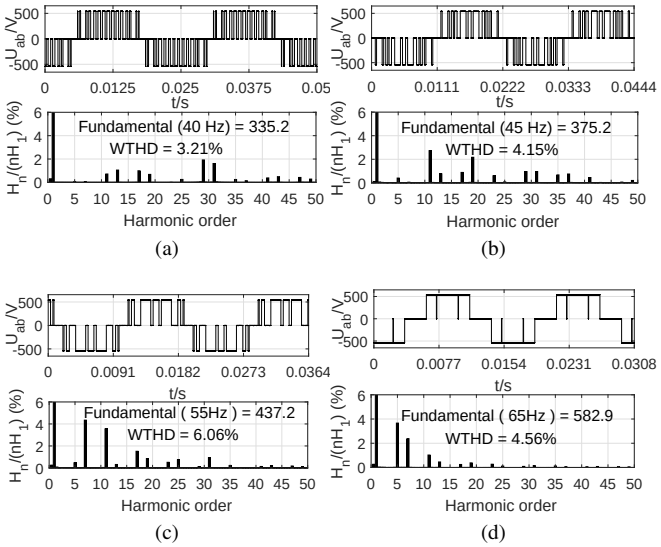

Fig. 11. Line voltage and corresponding WTHD for (a) SVPWM_15, (b) BBCS_11, (c) BBCS_7 and (d) SVPWM_3

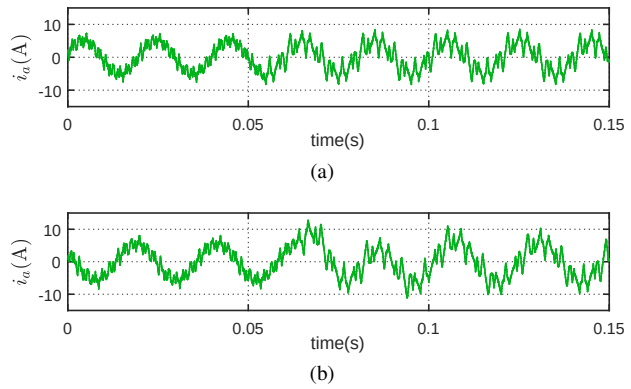

Fig. 12. Open loop test results of transition from BBCS_11 to BBCS_7 (a) with proposed method and (b) without proposed method

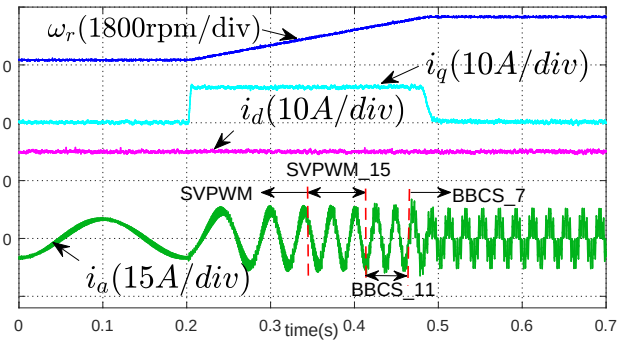

Fig. 13. Dynamic behavior of the machine in step speed command from 5 rpm to 1500 rpm

fast and smooth transition between different PWM schemes. The varying sampling rate with online correction is proposed to maintain symmetry of output voltage from the inverter during both dynamic and steady state operation. The whole scheme is experimentally verified on an induction motor drive platform. Both steady state and dynamic responses validate the effectiveness of proposed methods. As the modulation and

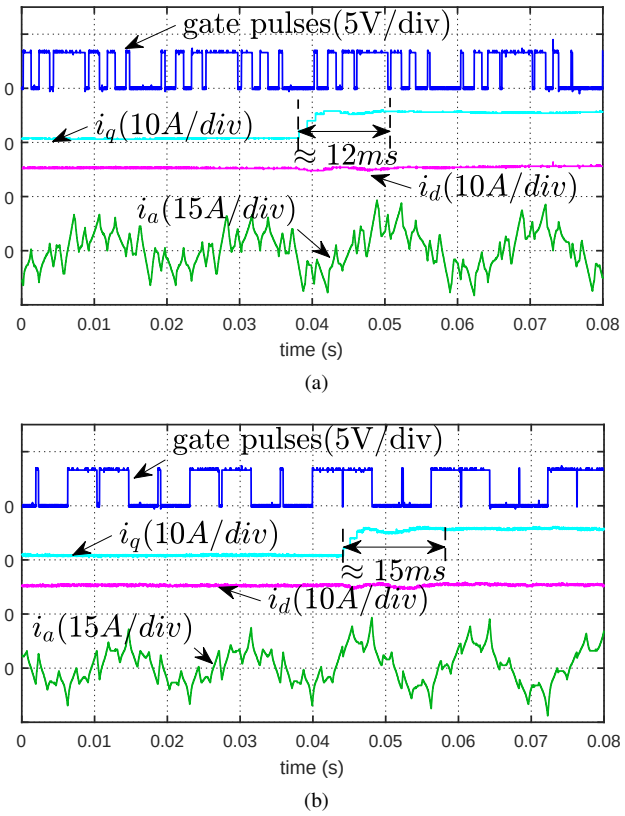

Fig. 14. i_q step responses for (a) BBCS_7 and (b) SVPWM_3

transition strategies are independent of machine model during both dynamic and steady process. The proposed method should be applicable to other types of machine with a well designed current controller.

REFERENCES

[1] J. Holtz and N. Oikonomou, "Fast dynamic control of medium voltage drives operating at very low switching frequency—an overview," *IEEE Trans. Ind. Electron.*, vol. 55, DOI 10.1109/TIE.2007.908540, no. 3, pp. 1005–1013, 2008.

[2] S. K. Sahoo and T. Bhattacharya, "Rotor flux-oriented control of induction motor with synchronized sinusoidal pwm for traction application," *IEEE Trans. Power Electron.*, vol. 31, DOI 10.1109/TPEL.2015.2475398, no. 6, pp. 4429–4439, Jun. 2016.

[3] G. Narayanan and V. T. Ranganathan, "Synchronised pwm strategies based on space vector approach. part 1: Principles of waveform generation," *IEE Proc.-Electr. Power Appl.*, vol. 146, DOI 10.1049/ip-epa:19990118, no. 3, pp. 267–275, May. 1999.

[4] Y. Zhang, D. Xu, C. Yan, and S. Zou, "Hybrid pwm scheme for the grid inverter," *IEEE J. Emerg. Sel. Topics Power Electron.*, vol. 3, DOI 10.1109/JESTPE.2015.2451159, no. 4, pp. 1151–1159, Dec. 2015.

[5] Y. Zhang, Z. Zhao, and J. Zhu, "A hybrid pwm applied to high-power three-level inverter-fed induction-motor drives," *IEEE Trans. Ind. Electron.*, vol. 58, DOI 10.1109/TIE.2010.2090836, no. 8, pp. 3409–3420, Aug. 2011.

[6] A. Mehrizi-Sani and S. Filizadeh, "An optimized space vector modulation sequence for improved harmonic performance," *IEEE Trans. Ind. Electron.*, vol. 56, DOI 10.1109/TIE.2008.2008997, no. 8, pp. 2894–2903, Aug. 2009.

[7] V. S. S. P. K. Hari and G. Narayanan, "Space-vector-based hybrid pwm technique to reduce peak-to-peak torque ripple in induction motor drives," *IEEE Trans. Ind. Appl.*, vol. 52, DOI 10.1109/TIA.2015.2487442, no. 2, pp. 1489–1499, Mar. 2016.

[8] G. Narayanan and V. T. Ranganathan, "Two novel synchronized bus-clamping pwm strategies based on space vector approach for high power drives," *IEEE Trans. Power Electron.*, vol. 17, DOI 10.1109/63.988673, no. 1, pp. 84–93, Jan. 2002.

[9] G. Narayanan and V. T. Ranganathan, "Synchronised pwm strategies based on space vector approach. part 2: Performance assessment and application to v/f drives," *IEE Proc.-Electr. Power Appl.*, vol. 146, DOI 10.1049/ip-epa:19990119, no. 3, pp. 276–281, May. 1999.

[10] J. Holtz and B. Beyer, "Fast current trajectory tracking control based on synchronous optimal pulsewidth modulation," *IEEE Trans. Ind. Appl.*, vol. 31, DOI 10.1109/28.464526, no. 5, pp. 1110–1120, 1995.

[11] Y. Wang, X. Wen, X. Guo, F. Zhao, and W. Cong, "Vector control of induction motor based on selective harmonic elimination pwm in medium voltage high power propulsion system," in *Int. Conf. Elect. Inf. and Cont. Eng.*, DOI 10.1109/ICEICE.2011.5777337, pp. 6351–6354, Apr. 2011.

[12] K. Yang, Z. Yuan, R. Yuan, W. Yu, J. Yuan, and J. Wang, "A groebner bases theory-based method for selective harmonic elimination," *IEEE Trans. Power Electron.*, vol. 30, DOI 10.1109/TPEL.2014.2388077, no. 12, pp. 6581–6592, Dec. 2015.

[13] R. Rathore, J. Holtz, and T. Boller, "Generalized optimal pulsewidth modulation of multilevel inverters for low-switching-frequency control of medium-voltage high-power industrial AC drives," *IEEE Trans. Ind. Electron.*, vol. 60, DOI 10.1109/TIE.2012.2217717, no. 10, pp. 4215–4224, 2013.

[14] Y. Wang, X. Wen, X. Guo, F. Zhao, and W.Cong, "The smooth transition research of different pwm modulations for vector control of induction motor in medium voltage high power," in *Int. Conf. Electr. Mach. and Syst.*, DOI 10.1109/ICEMS.2011.6073517, pp. 1–5, Aug. 2011.

[15] T. Geyer, N. Oikonomou, G. Papafotiou, and F. Kieferndorf, "Model predictive pulse pattern control," *IEEE Trans. Ind. Appl.*, vol. 48, DOI 10.1109/TIA.2011.2181289, no. 2, pp. 663–676, 2012.

[16] H. Kim, M. Degner, J. Guerrero, F. Briz, and R. Lorenz, "Discrete-time current regulator design for ac machine drives," *IEEE Trans. Ind. Appl.*, vol. 46, DOI 10.1109/TIA.2010.2049628, no. 4, pp. 1425 –1435, july-aug. 2010.

[17] G. Narayanan and V. T. Ranganathan, "Extension of operation of space vector pwm strategies with low switching frequencies using different overmodulation algorithms," *IEEE Trans. Power Electron.*, vol. 17, DOI 10.1109/TPEL.2002.802190, no. 5, pp. 788–798, Sep. 2002.

[18] B.-H. Bae and S.-K. Sul, "A compensation method for time delay of full-digital synchronous frame current regulator of PWM AC drives," *IEEE Trans. Ind. Appl.*, vol. 39, DOI 10.1109/TIA.2003.810660, no. 3, pp. 802–810, 2003.

[19] J. Holtz and N. Oikonomou, "Synchronous optimal pulsewidth modulation and stator flux trajectory control for medium-voltage drives," *IEEE Trans. Ind. Appl.*, vol. 43, DOI 10.1109/TIA.2006.889893, no. 2, pp. 600–608, 2007.

[20] M. Mengoni, L. Zarri, A. Tani, G. Serra, and D. Casadei, "A comparison of four robust control schemes for field-weakening operation of induction motors," *IEEE Trans. Power Electron.*, vol. 27, DOI 10.1109/TPEL.2011.2156810, no. 1, pp. 307 –320, jan. 2012.

[21] Y. Zhang, B. Xia, and H. Yang, "Performance evaluation of an improved model predictive control with field oriented control as a benchmark," *IET Electr. Power Appl.*, DOI 10.1049/iet-epa.2015.0614, May. 2016, to be published.

Haitao Yang (S'16) Haitao Yang received the B.S. degree from Hefei University of Technology, Hefei, China, in 2009 and the M.S. degree from North China University of Technology, Beijing, China, in 2015.

He is currently working toward the Ph.D. degree in the School of Electrical, Mechanical, and Mechatronic Systems, University of Technology, Sydney, NSW 2007, Australia. His research interests include motor drives, position/speed sensorless control of ac motors and high-performance traction drives.

Yongchang Zhang (M'10) received the B.S. degree from Chongqing University, China, in 2004 and the Ph.D. degree from Tsinghua University, China, in 2009, both in electrical engineering.

From August 2009 to August 2011, he was a Postdoctoral Fellow at the University of Technology Sydney, Australia. He joined North China University of Technology in August 2011 as an associate professor. Currently he is a full professor and the vice director of Inverter Technologies Engineering Research Center of Beijing. He has published more than 100 technical papers in the area of motor drives, pulsewidth modulation and AC/DC converters. His current research interest is model predictive control for power converters and motor drives.

Guofeng Yuan was born in Heilongjiang China, in 1979. He received the B.S. and Ph.D. degrees in electrical engineering from Tsinghua University, Beijing, in 2001 and 2006, respectively. From 2006 to 2008, he was an assistant professor with the Department of Electrical Engineering, Tsinghua University, Beijing, China. From 2008 to 2011, he was Chief Engineer with the Beijing Chino-Harvest Wind Power Technology Co. Ltd, Beijing, China. From 2011 to 2014, he was CTO with the Dalian GUOTONG Electrical Co. Ltd, Dalian, China. Since 2015, he has been a senior engineer with the Department of Electrical Engineering of North China University of Technology, Beijing, China. His research interests include control of electrical machines and converter for wind power generation system.

Paul D Walker was born in Sydney, Australia, in 1981. He received his B. E. in Mechanical Engineering from the University of Technology Sydney in 2007 and his PhD from the same university in 2011.

Since 2011 he has worked as a Research Associate and is currently a Chancellor's Postdoctoral Research Fellow at the School of Electrical, Mechanical and Mechatronic Systems at UTS. His research interests include the development of novel power splitting transmissions for hybrid electric vehicles, multi-speed transmission dynamics and control, and novel hybrid and electric vehicle topologies and their control.

Nong Zhang received PhD in 1989 from the University of Tokyo and worked at several universities in China, Japan, USA and Australia before joining University of Technology, Sydney in 1995. Since 2009, he has been the Professor of Mechanical Engineering, at School of Electrical, Mechanical and Mechatronic Systems, University of Technology Sydney. He focused on fundamental research on mechanical vibration, multi-body system dynamics and its applications to complex machines and vehicular systems. He developed advanced models and numerical schemes for simulating gear shift in powertrains with AT, MT and CVTs and for dynamic analysis of vehicles fitted with advanced suspensions.